





Addressing Fracture Properties of Individual Constituents Within a Cu-WTi-SiO_x-Si Multilayer

MARKUS ALFREIDER ^{1,3} JOHANNES ZECHNER,²
and DANIEL KIENER ¹

1.—Department of Materials Science, Chair of Materials Physics, Montanuniversität Leoben, Leoben, Austria. 2.—KAI Kompetenzzentrum Automobil- u. Industrieelektronik GmbH, Villach, Austria. 3.—e-mail: markus.alfreider@unileoben.ac.at

With modern materials applications continually decreasing in size, e.g., microelectronics, sensors, actuators, and medical implants, quantifying materials parameters becomes increasingly challenging. Specifically, addressing individual constituents of a system, such as interfaces or buried layers in a multilayer structure, emerges as a topic of great importance. We demonstrate herein a technique to assess fracture parameters of different interfaces of a Cu-WTi-SiO_x-Si model system based on in situ microcantilever testing in a scanning electron microscope. Positioning the initial notch position with respect to the interface of interest enabled selection of different crack paths, while an additional overlaid sinusoidal signal permitted continuous measurement of stiffness changes and thereby experimental measurement of the actual crack extension. We thus achieved continuous J - Δa curve measurements for the interface between Cu and WTi, the bulk WTi, and the interface between WTi and SiO_x. The localized nature of this novel approach makes it generally applicable to testing specific interfaces.

INTRODUCTION

Due to the continuous drive towards more powerful devices, a wide variety of modern materials applications rely on very small structural features. Depending on their application based on structural, semiconducting, or optical properties, this trend leads to an increasing number of different constituents confined to a very limited volume, such as multilayers or coatings of only a few tens to hundreds of nanometers in size. Experimentally addressing the individual properties of these constituents is rather challenging, but necessary as such nano- and microscale structures can exhibit drastically different properties compared with their bulk-like counterparts, if they even exist.¹ Specifically, the interface adhesion and fracture properties of such materials are a concern, as these characteristics could originate structural failure.² Microscale fracture mechanics is a rather recent field, with

varying approaches, such as double cantilever wedging,³ pillar splitting,⁴ or micro-cantilever bending as the most prominent geometries. However, most research in this field to date has been directed towards measuring single-phase fracture parameters of rather brittle materials, with only a few groups addressing interface properties. Matoy et al.⁵ studied the interfacial adhesion between SiO_x and Cu, W, or WTi using the cantilever deflection technique, while Schaufler et al.⁶ applied the same approach to study amorphous carbon coatings on steel substrates. However, due to the brittle nature of these materials, both groups were successfully able to apply linear elastic fracture mechanics concepts for the evaluation.⁷ Given that some components in applied systems can exhibit rather pronounced ductility, e.g., heat sinks or conductive layers (Cu, Al), those approaches are insufficient and it appears necessary to advance the field towards miniaturized elastic-plastic fracture mechanics concepts for interface testing. This will enable a better understanding of interface-controlled fracture processes for a wider group of materials.

In the present work, we utilize experiments based on the continuous J -integral measurement concept^{8,9} in situ inside a scanning electron microscope (SEM) and employ them on a Cu-WTi-SiO_x-Si multilayer model system, chosen as it combines materials with notable differences in elastic and plastic properties and thus providing an ideal test case for our elastic-plastic fracture methodology. Cantilever-shaped specimens manufactured from the layer stack were notched at different positions to address the crack extension behavior of the interface between SiO_x and WTi, the interface between WTi and Cu, and the WTi layer itself.

EXPERIMENTAL PROCEDURES

The model material system was synthesized on an 8-inch (001)-oriented Si wafer by first thermally growing amorphous SiO_x to a height of about 50 nm to 70 nm. Thereafter, a 270-nm- to 300-nm-thick WTi layer, as widely used in semiconductor and microelectromechanical systems (MEMS) fabrication, and a 300-nm Cu seed layer were deposited by magnetron sputtering. Using electrochemical deposition, an additional Cu layer was grown onto the seed, resulting in a total Cu thickness of 5 μm. Finally, the sample was annealed at 400°C for 30 min to ensure a stable microstructure at room temperature, resulting in a polycrystalline Cu film with grain size of ~ 2.7 μm. Further details can be found in Wimmer et al.¹⁰ and Bigl et al.¹¹ (refer to film A therein). Thereafter, the wafers were mechanically broken into 2 mm × 2 mm platelets, revealing the cross-sectional structure on a 90° edge, which enables further processing of the micron-sized specimens. The cantilevers were fabricated using a focused ion beam workstation (FIB, LEO 1540XB, Carl Zeiss AG, Oberkochen, Germany) situated at the edge of these platelets, as shown schematically in Fig. 1. To ensure a precise sample geometry, the ion beam current was subsequently reduced from 10 nA for coarse cuts to 50 pA for final polishing steps. The initial notch (a_0) was introduced as a through-thickness notch at the desired position (possibly close to the interfaces or within the WTi layer) before the final polishing step to minimize curtaining artifacts on the specimen surface.

The experiments were conducted inside the same FIB using a Hysitron PI-85 picoindenter (Bruker Corporation, Billerica, USA) equipped with a nanoDMA III upgrade to enable sinusoidal excitation for compliance measurements and a 5-μm-long conductive diamond wedge-shaped tip with opening angle of 60° (Synton-MDP AG, Nidau, Switzerland).

All the tests were conducted in open-loop mode at nominal speed of 10 μN/s, sinusoidal amplitude of 5 μN, and frequency of 80 Hz, based on previous work.⁹ The tests started from an initial contact load of 10 μN to reduce any issues with the inherently load-controlled transducer. The gathered data were

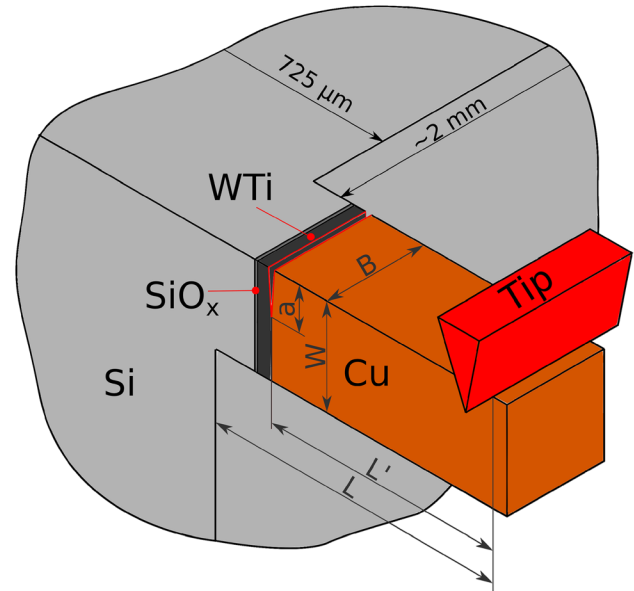


Fig. 1. Schematic of microcantilever testing geometry on the edge of a platelet showing the individual constituents as well as the geometric parameters (Color figure online).

evaluated using an approach similar to that used in Ref. 9, with some adjustments required due to the heterogeneous nature of the specimens as detailed below. First, the usual approach of splitting the J -integral into elastic and plastic parts and calculating iteratively, as suggested in ASTM 1820,¹² cannot be applied since no general elastic modulus E can be defined. Thus, we utilize an older form of the J -integral evaluation:^{13,14}

$$J_n = \frac{2A_{tot,n}}{B(W - a_n)} \quad (1)$$

where $A_{tot,n}$ is the total area under the load-displacement curve up to point n , B is the width and W is the height of the cantilever as shown in Fig. 1, and a_n is the crack length at point n . The respective crack length a_n was derived from the change in compliance signal following the formulation outlined in Ref. 15 as

$$\int_0^{a_n} \frac{a}{W} Y\left(\frac{a}{W}\right)^2 da = \frac{\left(\frac{k_0}{k_n} - 1\right)L^3}{18\pi(1 - \nu^2)L'^2} \quad (2)$$

where $Y(a/W)$ is a geometry factor, taken from Ref. 16, ν is the Poisson's ratio (taken as 0.3), W , L , and L' are geometric parameters shown in Fig. 1, k_0 is the stiffness of the unnotched beam, and k_n is the stiffness at point n . The stiffness in this case is inverse to the experimentally gathered dynamic compliance data. The integral in Eq. 2 was evaluated numerically using the trapezoidal rule, so that a_n was found by interpolation. The unnotched beam stiffness k_0 is dependent on the geometry of the

Table I. Geometry of individual cantilevers

	L (μm)	L' (μm)	B (μm)	W (μm)	a_0 (nm)	a_0/W	L'/L	L'/W
WTi-Cu interface	6.97 ± 0.04	4.06 ± 0.04	2.26 ± 0.04	2.06 ± 0.04	1259 ± 206	0.61	0.58	1.97
Inside WTi	6.79 ± 0.04	3.95 ± 0.04	1.29 ± 0.04	1.79 ± 0.04	1092 ± 76	0.61	0.58	2.01
WTi-SiO _x interface	7.34 ± 0.04	4.95 ± 0.04	1.79 ± 0.04	2.08 ± 0.04	1328 ± 70	0.64	0.67	2.38

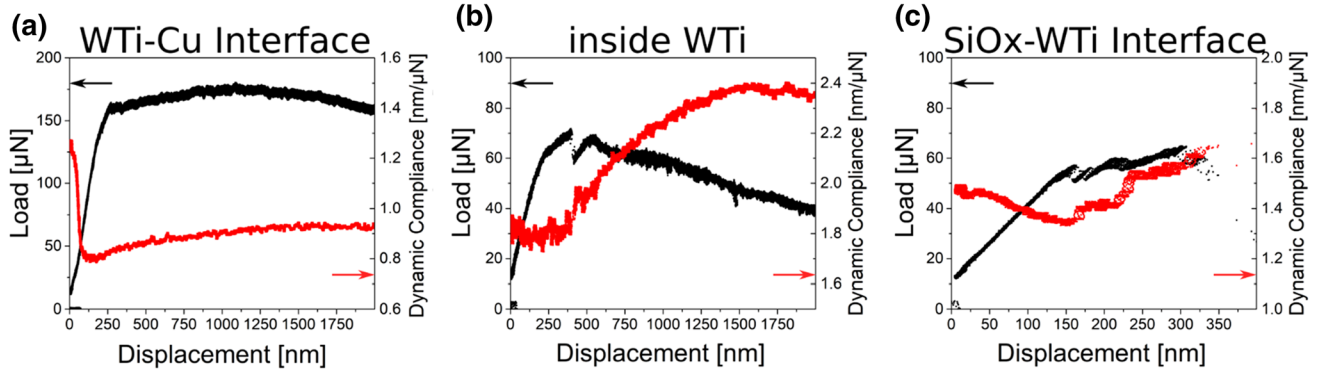


Fig. 2. Raw load–displacement data (black, left-hand side) and dynamic compliance data (red, right-hand side) of the individual specimens with notches (a) at the WTi-Cu interface, (b) inside the WTi, and (c) at the SiO_x-WTi interface (Color figure online).

specimen and the exact shape and elastic parameters of the individual constituents, making it challenging to evaluate. Therefore, we calculate k_0 from the initial stiffness of the notched cantilever $k(a_0)$ as

$$k_0 = k(a_0) \left(1 + \frac{18\pi(1 - \nu^2)L^2 a_0}{L^3} \int_0^a \frac{a}{W} Y\left(\frac{a}{W}\right)^2 da \right) \quad (3)$$

Note that Eqs. 2 and 3 are independent of specific materials parameters (with the exception of Poisson's ratio), as they consider a normalization by the stiffness of an unnotched cantilever. Thus, it is suggested that they are applicable also for heterogeneous materials systems as examined herein.

RESULTS

The geometry of the specimens was measured using ImageJ 1.54 s before deformation and is summarized in Table I. The error estimation for L , L' , B , and W are based on a measuring error of ± 5 pixels (± 40 nm), while the error estimation for the initial crack length a_0 is based on the standard deviation of 20 individual measurements conducted on the fracture surface after the experiment.

Since the goal was to compare cantilevers with different notch positions, it is necessary to keep the overall geometries identical, which is not always straightforward for micron-sized specimens. However, as shown in Table I, the ratios a_0/W , L'/L and L'/W are in very good agreement among the

different realizations, providing a strong indication that the observed behavior will be mainly dependent on the initial notch position.

In Fig. 2 the respective raw load–displacement data are shown on the left axis in black, while the dynamic compliance data are shown on the right axis in red. Due to slight variations in the sample geometry, the absolute values of the dynamic compliance can vary. However, it should be noted that the plotted range is kept constant at 1 nm/ μN for all three specimens to achieve better comparability, while the distinctly different levels of load and displacement required variable scaling of the axis. The data for the WTi-Cu interface (Fig. 2a) shows a load level exceeding 150 μN when the first strong deviation from linear behavior occurs, while these deviations are noticeable for the other two specimens at significantly lower levels, around 50 μN to 60 μN . Furthermore, the load in Fig. 2a increases up to a deflection of 1 μm , suggesting material hardening, whereas the load in Fig. 2b gradually decreases after an initial load drop at 360 nm. The dynamic compliance data for the WTi-Cu interface display a significant amount of initial contact compliance, down to a base level of 0.8 nm/ μN , and only a small increase in dynamic compliance during the experiment, while the data for the crack inside the WTi (Fig. 2b) shows only a small amount of initial contact compliance and a pronounced change of compliance during the experiment. Initial changes in compliance can be attributed to the establishment of a rigid contact between the indenter tip and cantilever and are a function of the

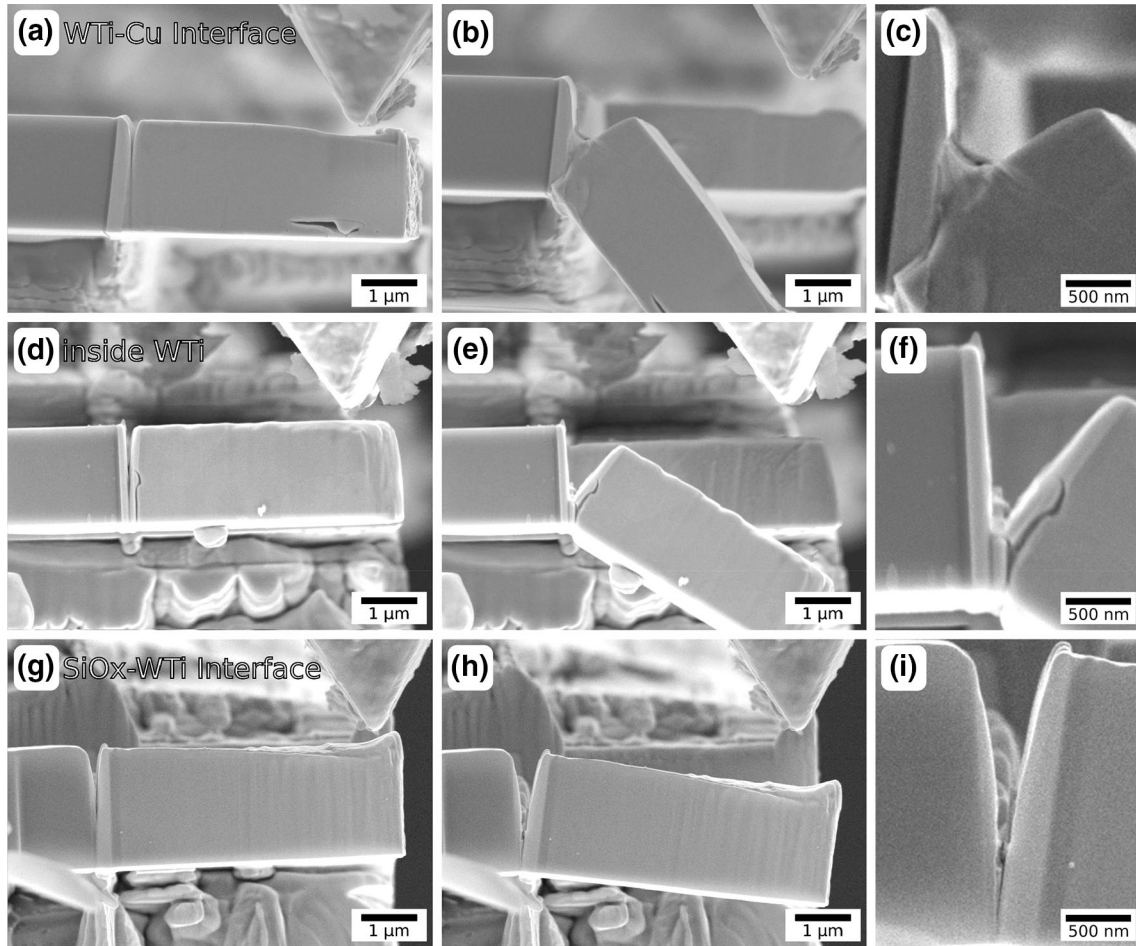


Fig. 3. In situ SEM images of the three cantilevers (a, d, g) before and (b, e, h) after deformation. (c, f, i) Magnifications of the notch position after deformation for a detailed view on the fracture/deformation process of the individual specimens.

individual material pairing, surface roughness, global stiffness of the specimen, and indentation plasticity. However, once contact is established during elastic loading of the beam, the overall cantilever compliance overtakes the contribution from the contact compliance, as is evident from the constant compliance level observed before the occurrence of plastic deformation or crack extension. The load–displacement curve for the SiO_x -WTi interface (Fig. 2c) depicts a stepwise behavior, suggesting that a crack forms at the notch tip and grows towards a feature, i.e., the interface, where it is stopped. This is further supported by the stepwise behavior of the matching dynamic compliance data.

Figure 3 depicts in situ SEM images of the individual specimens before and after testing. The WTi-Cu interface shows a major amount of plastic deformation, i.e., crack tip blunting in the Cu (Fig. 3b) but no obvious crack extension in the in situ images (Fig. 3c). This is in good accordance with the load and dynamic compliance data (Fig. 2a), respectively. The pore at the bottom of the cantilever in Fig. 3a as well as the hook-shaped edge of

the sample are FIB processing artifacts. However, the pore should not have a major influence, as its position is rather far away from the stress concentration produced by the notch, while the hook-shaped edge in connection with residual material on the wedge (Fig. 3a) is the most likely explanation for the strong change in contact compliance evident in the dynamic compliance data for this specimen (Fig. 2a). The sample with the notch inside the WTi (Fig. 3d) shows initial crack extension through the WTi layer, followed by a deflection of the crack front perpendicular towards the WTi-Cu interface, where again plastic deformation in the Cu governed the mechanical behavior and stopped further crack extension, as is evident from the decrease in dynamic compliance (Fig. 2b). The vertical feature at the interface between WTi and Cu is again a residual from FIB processing. However, as the crack grew initially inside the WTi, it is assumed to not act as a major defect influencing the fracture process. The specimen notched between WTi and SiO_x (Fig. 4g) exhibited the straightest crack extension without any visible plastic deformation.

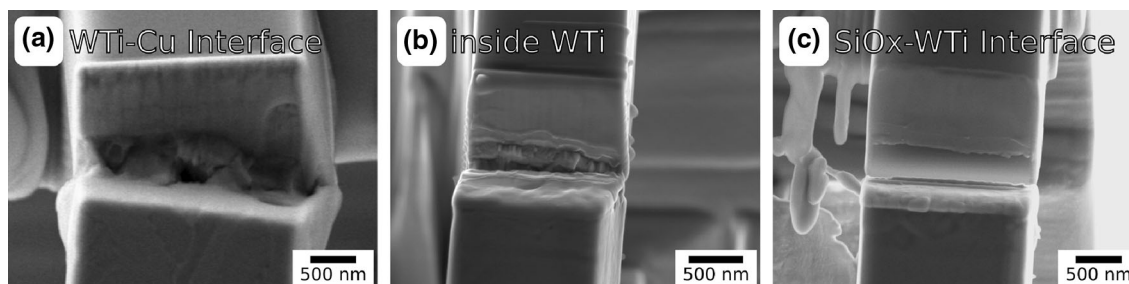


Fig. 4. Fracture surfaces of the (a) WTi-Cu interface, (b) WTi, and (c) SiO_x-WTi interface. All images taken under 30° tilt and in the direction towards the base of the cantilever.

Figure 4 shows the fracture surfaces under a tilt angle of 30° towards the base of each cantilever. From the WTi-Cu interface (Fig. 4a) it is evident that mainly plastic deformation has taken place, leading to the formation of a pore in the center of the fracture surface. Note that the cantilever was bent down further to achieve better visibility of the fracture surface after the actual experiment had ended. This resulted in a slight twist misalignment of the cantilever with respect to the crack front. In comparison, the fracture surface inside the WTi (Fig. 4b) shows short crack extension parallel to the interfaces, followed by perpendicular crack deflection towards the WTi-Cu interface. The faceted features at the origin of crack deflection suggest that it originated at WTi grain boundaries. Finally, the fracture surface of the SiO_x-WTi interface (Fig. 4c) depicts completely different features with perfectly straight crack extension starting from the initial notch through the connected ligament. The jagged line on the fracture surface suggests that the initial notch was not positioned perfectly at the interface, but rather in the WTi close to the interface. Thus, the crack had to grow towards the SiO_x-WTi interface before it accelerated in the interface, which is in good agreement with the stepwise load and dynamic compliance data (Fig. 2c) obtained during the testing of this specimen.

Figure 5a, b, and c depict the J -integral values calculated using Eq. 1 as a function of crack extension $\Delta a = a - a_0$ (Eq. 2) for all three specimens. The data at the bottom of the graph ($< 10 \text{ J/m}^2$, greyed area) show negative crack extension, which is only a measurement artifact due to the undefined increase in contact stiffness between the wedge tip and specimen in the early loading stages and should not be mistaken as physical crack extension. It is evident that the data for the WTi-Cu interface (Fig. 5a) as well as the data of the WTi notch (Fig. 5b) curve in the opposite direction to the behavior commonly observed in J - Δa analysis. Thus, they lie far outside any classical evaluation scheme for elastic-plastic fracture mechanics, as plasticity governs the majority of the deformation in these specimens. However, considering the detailed data shown in Fig. 5d and e, one can observe that

the first point of virtual crack extension exceeding 10 nm is around 23.6 J/m^2 for the WTi-Cu interface, while it is at about 51.2 J/m^2 for WTi. The J - Δa curve of the SiO_x-WTi interface (Fig. 5c and f) shows two steps of rapid crack extension at 12.1 J/m^2 and 18.2 J/m^2 before the final unstable crack extension at 32.4 J/m^2 , after which J increases approximately linearly with Δa .

DISCUSSION

It is clearly evident from the in situ images as well as the J - Δa data that all three specimens show distinctly different behavior with regards to the interplay between crack extension and plastic deformation. The WTi-Cu interface specimen shows no resemblance to classical fracture mechanics, where the initial crack tip blunting, visible as an increasing J -integral at an approximately constant initial crack length a_0 would be followed by evident crack extension, resulting in a concave-down shape (negative second derivative) of the J - Δa curve. Instead, the measured compliance increases nearly instantly (Fig. 2a), resulting in an immediate increase in the calculated crack extension (Fig. 5a and d) and a concave-up shape of the J - Δa curve. However, as evident from the in situ images (Fig. 3b and c), this only corresponds to a major amount of plastic deformation, resulting in crack tip blunting right from the start of the experiment. On the other hand, the specimen with the notch inside the WTi exhibits a more classical behavior with loading up to 51.2 J/m^2 (Fig. 5e) before a crack extension higher than 20 nm is detected. This suggests that the initial behavior is driven to a larger extent by fracture through the WTi layer, before plasticity finally takes over once the crack deviates into the WTi-Cu interface. Considering an elastic modulus for WTi of $E = 324 \text{ GPa}$,⁵ a J -integral value of 51.2 J/m^2 corresponds to a stress intensity factor $K = \sqrt{JE}$ of $4.1 \text{ MPa m}^{1/2}$ (in-plane stress loading condition). Studies on single-crystalline W of similar size and with elastic-plastic considerations in mind showed stress intensities between $3 \text{ MPa m}^{1/2}$ and $16 \text{ MPa m}^{1/2}$,^{9,17,18} depending on the orientation, size, and exact evaluation criterion. However,

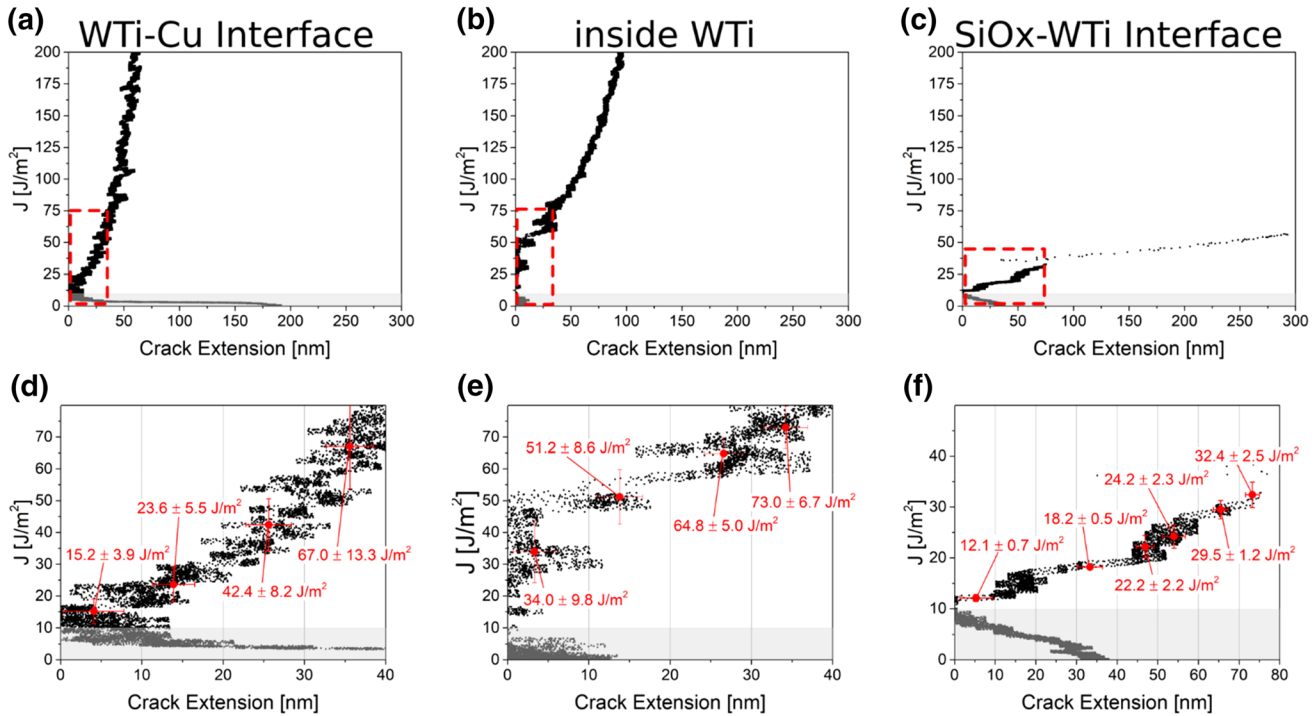


Fig. 5. J - Δa curves of the individual specimens: (a) WTi-Cu interface, (b) WTi, and (c) SiO_x-WTi interface. The details marked with red boxes are shown below (d–f) with the red marks being averaged data in the respective 10-nm-wide windows (Color figure online).

considering that the WTi layer is synthesized by sputter deposition, which commonly results in grain sizes of tens of nanometers,¹⁹ the contribution of grain boundaries and their respective interface toughness cannot be neglected. Therefore, the observed value of $4.1 \text{ MPa m}^{1/2}$ lies at the lower end of the range in comparison with single-crystalline W. Treml et al.²⁰ studied a multilayer stack consisting of sputtered W and Cu with film thickness similar to the WTi in the present experiments, finding a fracture toughness of $3.3 \text{ MPa m}^{1/2}$. Taking into account that their experimental setup allowed for crack propagation along the columnar grain boundaries obtained by sputter deposition, while the geometry used herein constrains the crack to grow perpendicular to the columns, a slightly higher fracture toughness is expected.²¹ Furthermore, one has to mention that the creation of the notch by FIB processing can lead to an undefined, higher defect density at the notch ground,²² which could promote the initial crack extension through the WTi layer. Since the crack deflects along the weaker columnar boundaries as shown in Fig. 4b, it is not possible to distinguish whether the initial crack growth is a result of the local position of the initial notch (inside the grains) or the FIB damage. However, in comparison with literature, the obtained value seems reasonable and gives us confidence that the calculated initiation of crack extension is mainly due to material fracture processes. The SiO_x-WTi specimen shows the greatest resemblance to classical fracture mechanics, as it is the only specimen with unstable crack growth.

However, the initial two steps in the J - Δa data (Fig. 5f) suggest that a crack nucleus was forming at the interface prior to final failure. Therefore, the interface toughness should not be taken as the maximum J , but rather as the difference between the maximum J before final failure and the last plateau that suggests crack initiation, such that $J_{\text{interface}} = 32.4 - 18.2 = 14.2 \text{ J/m}^2$. Matoy et al.⁵ reported an interface toughness for their SiO_x-WTi interface of $G = 4.8 \text{ J/m}^2$, with $G = J$ in the linear elastic case. This value seems to be quite low in comparison with our elastic-plastic result, especially as no strong evidence of plastic deformation is present in the SiO_x-WTi specimen (Figs. 3h and i, 4c). Calculating the linear elastic energy release rate for the given specimen as presented in Ref. 5, with a maximum load of $F = 64.7 \text{ }\mu\text{N}$ (Fig. 2-c) results in $G = 2.9 \text{ J/m}^2$, which is in the same range as their results. However, Matoy et al. took a constant geometry factor of 1.12, which is known to be valid only for very deep notches in a semi-infinite plate, loaded in pure tension (mode I).²³ Considering that the geometry factor shows a rather different dependence in the used cantilever-shaped geometry, as shown by Brinkmann et al.,²⁴ one can recalculate the linear elastic energy release rate from Matoy et al.⁵ to be $G = 11.0 \text{ J/m}^2$, when using the more appropriate geometry factor taken from Ref. 16. This appears to be in good agreement with the observed amount of $J = 14.2 \text{ J/m}^2$, in particular when taking into account differences in chemistry and some minor contribution of plasticity.

While the distinctive difference between all three samples is evident, it should be noted that the quantitative values should be taken with care, as the measurements are in a regime where the classical criteria for size-independent fracture properties are no longer valid. Furthermore, as only three or four Cu grains are in contact with the WTi interface, their specific crystallographic orientations could have a distinct influence. However, full tomographic analysis of each specimen would be necessary to address the individual orientational dependencies, which lies beyond the scope of this work. Furthermore, the experiments as conducted herein (based on load–displacement data) measure the global change of the J -integral and are not capable of resolving the fluctuations in the near field surrounding the crack tip, which are governed by the elastic and plastic incompatibilities of the individual constituents. Nevertheless, as the size of the features in microelectronic components is in the dimensional range considered herein, the obtained values can be considered valid as the experiments were conducted at the native scale of the features of interest. Thus, the presented experimental approach can act as a method to generate input for further analysis of microelectronic components or other miniaturized features.

CONCLUSION

Different interfaces of a Si-SiO_x-WTi-Cu multilayer were successfully measured by the micro-cantilever deflection technique. The WTi-Cu interface showed no resemblance to classical fracture mechanics concepts, but rather a distinct contribution of plastic deformation. However, as the geometry applied allowed for very local probing of this interface, no other interface reached a critical stress intensity, which is very promising for probing individual features with higher toughness close to others with lower toughness. For the SiO_x-WTi interface, we demonstrated the possibility to nucleate a natural crack from an FIB notch prior to final failure. This again is very promising for specimens that are known to be influenced by FIB processing. Furthermore, the resulting interface toughness of 14.2 J/m² is in excellent agreement with previously conducted experiments when properly analyzing those. Beyond interface toughness experiments, it was also shown that, by careful positioning the initial notch, even the only 300-nm-thick WTi layer could be investigated, resulting in a fracture toughness of $J = 51.2 \text{ J/m}^2$ ($K = 4.1 \text{ MPa m}^{1/2}$), which is again in good agreement with literature values for sputtered W. Therefore, these results give confidence that carefully executed micro-cantilever deflection experiments in conjunction with proper elastic–plastic fracture mechanics considerations can be utilized to address quantitative, if not always size-independent, local fracture properties of specific phases and interfaces.

ACKNOWLEDGEMENTS

The authors gratefully acknowledge the financial support under the scope of the COMET program within the K2 Center Integrated Computational Material, Process and Product Engineering (IC-MPPE) project A2.12. This program is supported by the Austrian Federal Ministries for Transport, Innovation, and Technology (BMVIT) and for Digital and Economic Affairs (BMDW), represented by the Österreichische Forschungsförderungsgesellschaft (funder ID <https://doi.org/10.13039/501100004955>), and the federal states of Styria, Upper Austria, and Tyrol. Furthermore, this project has received funding from the European Research Council (ERC) under the European Union's Horizon 2020 research and innovation program (Grant No. 771146 TOUGHIT).

FUNDING

Open access funding provided by Montanuniversität Leoben.

CONFLICT OF INTEREST

On behalf of all authors, the corresponding author states that there are no conflicts of interest.

OPEN ACCESS

This article is licensed under a Creative Commons Attribution 4.0 International License, which permits use, sharing, adaptation, distribution and reproduction in any medium or format, as long as you give appropriate credit to the original author(s) and the source, provide a link to the Creative Commons licence, and indicate if changes were made. The images or other third party material in this article are included in the article's Creative Commons licence, unless indicated otherwise in a credit line to the material. If material is not included in the article's Creative Commons licence and your intended use is not permitted by statutory regulation or exceeds the permitted use, you will need to obtain permission directly from the copyright holder. To view a copy of this licence, visit <http://creativecommons.org/licenses/by/4.0/>.

REFERENCES

1. M.D. Uchic, D.M. Dimiduk, J.N. Florando, W.D. Nix, *Science* 305, 986 (2004).
2. J. Berger, O. Glushko, V.M. Marx, C. Kirchlechner, and M.J. Cordill, *JOM* 68, 1640 (2016).
3. G. Sernicola, T. Giovannini, P. Patel, J.R. Kermode, D.S. Balint, T. Ben Britton, and F. Giuliani, *Nat. Commun.* 8, 108 (2017).
4. M. Sebastiani, K.E. Johanns, E.G. Herbert, F. Carassiti, and G.M. Pharr, *Philos. Mag.* 95, 1928 (2015).
5. K. Matoy, T. Detzel, M. Müller, C. Motz, and G. Dehm, *Surf. Coat. Technol.* 204, 878 (2009).
6. J. Schaufner, C. Schmid, K. Durst, and M. Göken, *Thin Solid Films* 522, 480 (2012).
7. R. Pippan, S. Wurster, and D. Kiener, *Mater. Des.* 159, 252 (2018).

8. J. Ast, B. Merle, K. Durst, and M. Göken, *J. Mater. Res.* 31, 3786 (2016).
9. M. Alfreider, D. Kozic, O. Kolednik, and D. Kiener, *Mater. Des.* 148, 177 (2018).
10. A. Wimmer, M. Smolka, W. Heinz, T. Detzel, W. Robl, C. Motz, V. Eyert, E. Wimmer, F. Jahnel, R. Treichler, and G. Dehm, *Mater. Sci. Eng. A* 618, 398 (2014).
11. S. Bigl, S. Wurster, M.J. Cordill, and D. Kiener, *Thin Solid Films* 612, 153 (2016).
12. ASTM Standard E1820, *Standard Test Method for Measurement of Fracture Toughness* (West Conshohocken, USA, 2013).
13. J.R. Rice, P.C. Paris, and J.G. Merkle, *Progress in Flaw Growth and Fracture Toughness Testing*, ed. J. Kaufman, J. Swedlow, H. Corten, J. Srawley, R. Heyer, E. Wessel, and G. Irwin (West Conshohocken: ASTM International, 1973), pp. 231–245.
14. X.K. Zhu and J.A. Joyce, *Eng. Fract. Mech.* 85, 1 (2012).
15. M. Alfreider, S. Kolitsch, S. Wurster, and D. Kiener, *Mater. Des.* 194, 108914 (2020).
16. A. Riedl, R. Daniel, M. Stefanelli, T. Schöberl, O. Kolednik, C. Mitterer, and J. Keckes, *Scr. Mater.* 67, 708 (2012).
17. J. Ast, M. Göken, and K. Durst, *Acta Mater.* 138, 198 (2017).
18. S. Wurster, C. Motz, and R. Pippan, *Philos. Mag.* 92, 1803 (2012).
19. F. Saghaeian, J. Keckes, S. Woehlert, M. Rosenthal, M. Reisinger, and J. Todt, *Thin Solid Films* 691, 137576 (2019).
20. R. Treml, D. Kozic, R. Schöngrundner, O. Kolednik, H.P. Gänser, R. Brunner, and D. Kiener, *Extreme Mech. Lett.* 8, 235 (2016).
21. R. Daniel, M. Meindlhumer, W. Baumeegger, J. Todt, J. Zalesak, T. Ziegelwanger, C. Mitterer, and J. Keckes, *Mater. Des.* 161, 80 (2019).
22. D. Kiener, C. Motz, M. Rester, M. Jenko, and G. Dehm, *Mater. Sci. Eng. A* 459, 262 (2007).
23. T.L. Anderson, *Fracture Mechanics: Fundamentals and Applications*, 2nd ed. (Boca Raton: CRC Press, 2005).
24. S. Brinckmann, K. Matoy, C. Kirchlechner, and G. Dehm, *Acta Mater.* 136, 281 (2017).

Publisher's Note Springer Nature remains neutral with regard to jurisdictional claims in published maps and institutional affiliations.